Applied Physics Express

The Japan Society of Applied Physics

LETTER • OPEN ACCESS

Prospects of mist CVD for fabrication of β-Ga_2O_3 MESFETs on β-Ga_2O_3 (010) substrates

To cite this article: Hitoshi Takane *et al* 2023 *Appl. Phys. Express* **16** 081004

OPEN ACCESS
Applied Physics Express **16**, 081004 (2023) **LETTER**
https://doi.org/10.35848/1882-0786/acefa5

Prospects of mist CVD for fabrication of β-Ga_2O_3 MESFETs on β-Ga_2O_3 (010) substrates

Hitoshi Takane[1], Yuji Ando[2,3], Hidemasa Takahashi[3], Ryutaro Makisako[3], Hikaru Ikeda[4], Tetsuzo Ueda[5], Jun Suda[2,3], Katsuhisa Tanaka[1], Shizuo Fujita[4*], and Hidetaka Sugaya[6*]

[1]Department of Material Chemistry, Kyoto University, Kyoto 615-8510, Japan
[2]Institute of Materials and Systems for Sustainability, Nagoya University, Nagoya 464-8601, Japan
[3]Department of Electronics, Nagoya University, Nagoya 464-8601, Japan
[4]Office of Society-Academia Collaboration for Innovation, Kyoto University, Kyoto 606-8501, Japan
[5]Panasonic Industry Co., Ltd., Kadoma 571-8506, Japan
[6]Living Appliances and Solutions Company, Panasonic Corporation, Tokyo 105-8301, Japan

*E-mail: fujitasz@kuee.kyoto-u.ac.jp; sugaya.hidetaka@jp.panasonic.com

Received June 28, 2023; revised August 4, 2023; accepted August 10, 2023; published online August 29, 2023

Mist CVD was applied to grow the β-Ga_2O_3 channel layer of a MESFET on a semi-insulating β-Ga_2O_3 (010) substrate. The mobility and carrier concentration of the channel layer were 80 $cm^2\ V^{-1}\ s^{-1}$ and $6.2 \times 10^{17}\ cm^{-3}$, respectively. The device exhibited a pinch-off characteristic with a threshold gate voltage of −9 V, and the maximum drain current was 240 mA mm^{-1}. The maximum transconductance was 46 mS mm^{-1} and the on-resistance was 30 Ω mm. This device performance suggests that mist CVD is a potential growth technology capable of providing low-cost devices in the future.

β-Ga_2O_3, an ultra-wide bandgap semiconductor, is one of the promising materials for fast, compact, and energy-efficient power-electronic devices due to its large bandgap of 4.5–4.9 eV and high electric breakdown field of 6–8 MV cm^{-1}, which exceed those of conventional Si, SiC, and GaN.[1,2] These features enable further compact devices with low on-state resistances and high breakdown voltages. One of its advantages is that high-quality β-Ga_2O_3 single-crystal wafers can be synthesized by atmospheric melt-growth techniques,[3–7] and this has allowed device-quality homoepitaxial growth of β-Ga_2O_3 by molecular beam epitaxy (MBE),[8,9] halide vapor phase epitaxy (HVPE),[10] and metal-organic CVD (MOCVD).[11] To date, various β-Ga_2O_3 devices, such as Schottky barrier diodes (SBDs),[12–14] heterojunction pn diodes,[15,16] and lateral and vertical transistors including MESFETs,[17–20] MOSFETs,[21–24] and modulation-doped FETs (MODFETs),[25–28] have been intensively demonstrated.

Mist CVD, which has been developed for the growth of oxide thin films,[29–33] is another candidate of the growth technology for β-Ga_2O_3 devices. This technology uses a simple and non-vacuum apparatus, and a water/alcohol solution of metal compounds as a precursor, which enables safe, cost-effective, energy-saving, and highly scalable growth. There have been some reports on homoepitaxial growth of β-Ga_2O_3 and coherent growth of β-$(Al_xGa_{1-x})_2O_3$ alloys by the mist CVD.[34–37] Conductivity control by Sn- and Ge-doping of homoepitaxial β-Ga_2O_3 was also achieved with carrier concentrations on the order of $10^{17}\ cm^{-3}$.[34,36] Following this, it is important to demonstrate device fabrication by mist CVD method for future mass production and from the viewpoint of sustainable development goals (SDGs). In this letter, we report the fabrication of β-Ga_2O_3 MESFETs with the use of mist CVD on single-crystal β-Ga_2O_3 (010) substrates and the demonstration of the device performance to show the prospects of mist CVD for cost-effective practical devices.

Before fabricating β-Ga_2O_3 MESFETs, we examined the basic growth characteristics of β-Ga_2O_3 homoepitaxial films on β-Ga_2O_3 substrates. The growth was performed by a homemade hot-wall-type mist CVD system on β-Ga_2O_3 (010) substrates (Novel Crystal Technology Inc.). Si was adopted as an n-type dopant. Figure 1 shows the schematics of the mist generator. For Ga and Si precursors, we chose tris (acetylacetonato)gallium (III) and chloro-(3-cyanopropyl)-dimethylsilane, respectively, which were dissolved in deionized water with the addition of a few amounts of hydrochloric acid. Hydrochloric acid was necessary to completely dissolve the precursors in the aqueous solution. Ga concentration in the aqueous solution was set at 0.05 mol l^{-1} and [Si]/[Ga] ratio in the solution was changed between 1×10^{-6} and 2×10^{-4} to control the carrier (electron) concentration in n-type Ga_2O_3 layers. The source aqueous solution was installed in the mist generator shown in Fig. 1, and was atomized using ultrasonic transducers. The precursor mist was supplied to a horizontal quartz reactor heated at 700 °C–800 °C using O_2 carrier and dilution gases. The carrier and dilution gas flow rates were set at 3.0 and 0.5 l min^{-1}, respectively. For the growth of Ga_2O_3, the water and/or the O_2 gas act as an oxygen source. Prior to the homoepitaxy, the β-Ga_2O_3 substrates were cleaned using acetone, ethanol, and deionized water.

The electrical properties, thicknesses, and structural properties of the epilayers were evaluated by Hall effect measurements, surface profile measurements, and X-ray diffraction (XRD) measurements, respectively. As ohmic contacts for the Hall effect measurement, Ti/Au electrodes with Van der Pauw configuration were prepared by electron beam evaporation.

Figure 2(a) indicates the growth rate of the mist CVD-grown β-Ga_2O_3 homoepitaxial films on β-Ga_2O_3 (010) substrates. The growth rate decreased at higher growth temperatures, which was consistent with the reports by Lee et al.[34] and Nishinaka et al.[35] This trend can be

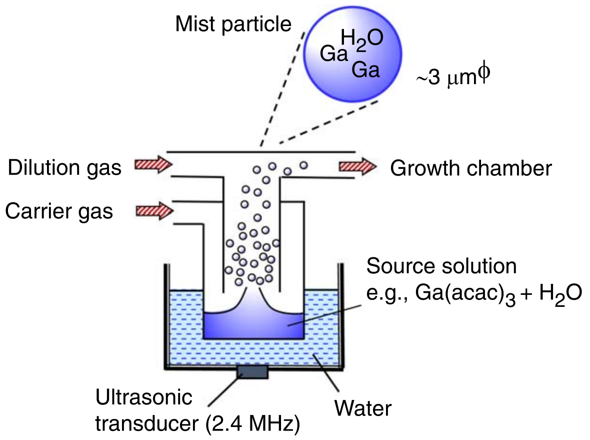

Fig. 1. Schematics of the mist generator used for mist CVD growth. Mist particles contain Ga elements, H_2O, and their intermediate formations. The ultrasonic frequency is 2.4 MHz, where the diameter of spherical mist particles is around 3 μm.

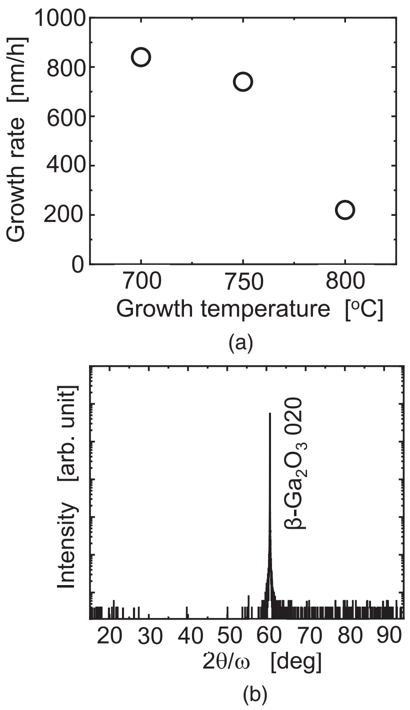

Fig. 2. (a) Growth rate of the mist CVD-grown β-Ga_2O_3 homoepitaxial layers on β-Ga_2O_3 (010) substrates. (b) XRD symmetric $2\theta/\omega$ scan profile of a Si-doped β-Ga_2O_3 layer ([Si]/[Ga] $= 1 \times 10^{-6}$ in the source solution).

attributed to the fact that at higher temperatures precursors were preferentially consumed in the gas phase and at the tube wall before being transported onto the substrate.[34,35] In this study, we temporarily adopted 750 °C as the growth temperature since a reasonable growth rate was obtained as shown in Fig. 2(a). Nevertheless, the growth rate of 750 nm h^{-1} at 750 °C is much lower than the highest value of 3.2 μm h^{-1} reported by Nishinaka et al.,[35] because the Ga concentration in the source solution was lower. For Si-doping, the electron concentrations were controlled in the order of 10^{17} to 10^{19} cm^{-3}. The actual electronic properties of the MESFET channel layer were measured using the test elementary group (TEG) pattern in the device. Figure 2(b) shows the XRD symmetric $2\theta/\omega$ scan profile of a Si-doped epilayer ([Si]/[Ga] $= 1 \times 10^{-6}$ in the source solution). Any

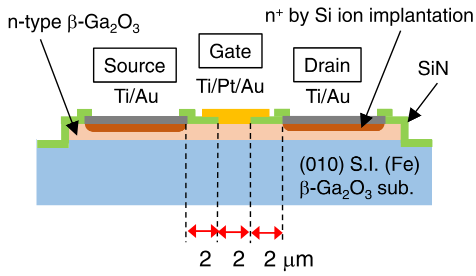

Fig. 3. Cross-sectional schematic image of the β-Ga_2O_3 MESFET structure.

peaks derived from other plane orientations of β-Ga_2O_3 and other polymorphs of Ga_2O_3 were not observed, suggesting the formation of a single-phase β-Ga_2O_3 epilayer.

β-Ga_2O_3 MESFETs were fabricated by using Si-doped mist CVD-grown epilayers as the channel layers on Fe-doped semi-insulating β-Ga_2O_3 (010) substrates (10 $\times$ 15 mm^2). The device fabrication processes were conducted at the Center for Integrated Research of Future Electronics–Transformative Electronics Facilities (C-TEFs) at Nagoya University. Figure 3 shows the cross-sectional schematic image of the MESFETs fabricated in this study. In the actual process, first, a 200 nm thick Si-doped β-Ga_2O_3 epilayer was grown by mist CVD ([Si]/[Ga] $= 1 \times 10^{-6}$ in the source solution) on a Fe-doped semi-insulating β-Ga_2O_3 (010) substrate. The mesa structure was formed by using conventional photolithography and inductively coupled plasma-reactive ion etching (ICP-RIE) using BCl_3/Cl_2. Si implantations were performed to form source and drain regions with a 200 nm deep box profile and total Si dose of 2.0×10^{15} cm^{-2} (target Si density $= 1 \times 10^{20}$ cm^{-3}), followed by 30-min activation annealing at 925 °C in N_2 gas. On the source and drain regions, a Ti(20 nm)/Au(230 nm) metal stack was deposited and then annealed at 470 °C as the source and drain electrodes. We had already established the process conditions for the fabrication of n^+-regions and their electrodes using the unintentionally-doped β-Ga_2O_3 layers grown by molecular beam epitaxy (MBE). The transfer length measurements (TLM) on the highly Si-doped layer ($\sim 1 \times 10^{20}$ cm^{-3}) had revealed the contact resistance R_c of 0.32 Ω mm and the specific contact resistance ρ_c of the order of 10^{-6} Ω cm^2. In the present experiments for the mist CVD-grown β-Ga_2O_3, we adopted the process conditions ever established.

A 60 nm thick SiN passivation layer was fabricated by PECVD. For the gate region, after the SiN passivation layer was etched off by ICP-RIE using SF_6, a Ti (3 nm)/Pt (12 nm)/Au (350 nm) metal stack was deposited. Finally, a SiN passivation layer was etched by ICP-RIE using CF_4 for the contact to source and drain regions. The use of SF_6 for forming the gate, rather than CF_4, is because we expected less damage to the β-Ga_2O_3 layer, where the Schottky electrode is subsequently formed (not confirmed by experiments). The gate-to-source length (L_{GS}), gate-to-drain length (L_{GD}), gate length (L_G), field-plate extension of the gate toward the source (L_{FP_S}) and that toward the drain (L_{FP_D}) were 2, 2, 2, 1, and 1 μm, respectively. The gate width (W_G) was 50 μm.

The Hall effect measurement using the Van der Pauw TEG pattern in the device revealed the mobility, sheet carrier density, and sheet resistance of the channel layer as 80 cm^2 V^{-1} s^{-1}, 1.24×10^{13} cm^{-2}, and 6.2 kΩ sq^{-1},

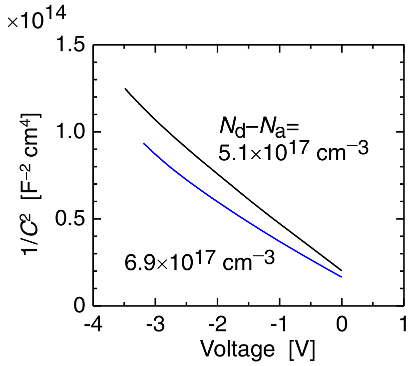

Fig. 4. Capacitance–voltage characteristics of the two Schottky contacts formed on the channel layer at different positions as the $1/C^2$–V plot.

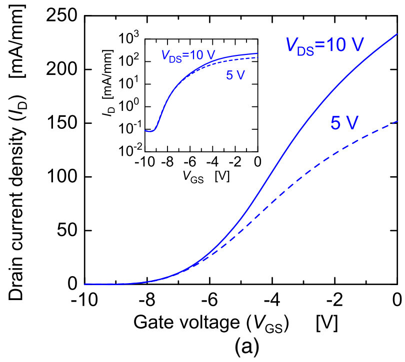

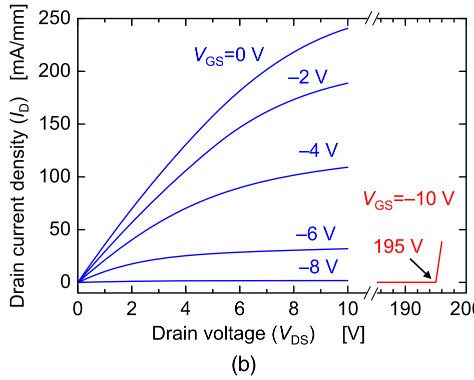

Fig. 5. Electrical properties of the fabricated β-Ga_2O_3 MESFET. Drain current density I_D versus (a) the gate–source voltage V_{GS} and (b) the drain–source voltage V_{DS} for the different gate–source voltage V_{GS}. In (a), the inset is the log plot of I_D.

respectively. From the thickness of the channel layer (200 nm), the carrier concentration was calculated as $6.2 \times 10^{17}\ cm^{-3}$. The Hall mobility is comparable to or only slightly lower than those of β-Ga_2O_3 homoepitaxial layers at the similar carrier concentration grown by MBE and MOCVD.[38] This fact suggests that our β-Ga_2O_3 channel layer has sufficient quality for electronic devices.

Figure 4 shows the capacitance–voltage (C–V) characteristics of two Schottky contacts (200 μm in diameter) formed on the channel layer at different positions. From the average slopes of the linear regions of $1/C^2$ versus V in this graph, the effective donor concentration $N_d - N_a$ was revealed as 5.1 or $6.9 \times 10^{17}\ cm^{-3}$ using the relative permittivity of 10.[39] This supports the carrier concentration of $6.2 \times 10^{17}\ cm^{-3}$ obtained by the Hall effect measurement within the experimental error or potion-to-potion variation.

The electrical properties of the MESFET are shown in Fig. 5. Figure 5(a) shows the drain current density I_D versus the gate–source voltage V_{GS} of the MESFET. The log plot of I_D is shown in the figure inset of the linear plot. Here, the drain–source voltage V_{DS} was kept at 5 or 10 V. The modulation of I_D with V_{GS} was seen and a pinch-off characteristics was observed at a threshold gate voltage of $V_{GS} = -9$ V. The maximum transconductance g_m was 46 mS mm^{-1}. However, I_D did not drop lower than 0.08 mA mm^{-1} and several devices did not show clear pinch-off. Therefore, we should say that current leakage at the n-Ga_2O_3/substrate interface is not sufficiently suppressed. Since the n-Ga_2O_3 layer was directly grown on the substrate without a buffer layer, Si may have accumulated at the interface and contributed as a leakage path.[40] It is also possible that Fe diffuses from the substrate to the n-Ga_2O_3 layer.[41] Efforts to overcome these phenomena will continue to improve device performance in the future.

The DC drain characteristics, that is, the relationships between the drain current density I_D versus the drain–source voltage V_{DS} for the different gate–source voltage V_{GS} as parameters are shown in Fig. 5(b). In the measurement range, the maximum I_D was 240 mA mm^{-1}. The on-resistance was found to be $R_{ON} = 30\ \Omega$ mm. The off-state breakdown under $V_{GS} = -10$ V occurred at $V_{DS} = 195$ V. To increase the breakdown voltage as well as to reduce the on-state resistance, we will optimize the device structure and the growth conditions in further study.

Mist CVD is a simple, safe, cost-effective, and energy-saving growth technology. Now it is hard for most CVD to achieve the control of low carrier concentrations, such as the order of $10^{16}\ cm^{-3}$ (this is pointed out not only in our study but also by Ogawa et al.[36]), which has been easily attained by MBE and MOCVD. One reason for this may be that the source precursors currently used in mist CVD are commercially available chemicals that have not been purified to meet semiconductor grade, leaving any unintentional impurities in the film. It is also possible that Si in the quartz tube decomposes in the water and hydrogen-containing environment of mist CVD and is incorporated into the grown film, as suggested by Konishi et al.[42] in the halide vapor phase epitaxy of β-Ga_2O_3. Efforts for solving these problems will be continued. Nevertheless, it was found that for the β-Ga_2O_3 layers of the carrier concentration of the order of high $10^{17}\ cm^{-3}$, mist CVD can compete with sophisticated growth technologies such as MBE and MOCVD in the film quality. Applications of the films as devices are investigated in the present work, and the performance of MESFETs was not inferior or might be superior to those grown by MBE or MOCVD.

In summary, in this letter, we showed the performance of β-Ga_2O_3 MESFETs whose active layer was grown by the simple, safe, cost-effective, and energy-saving growth technology of mist CVD. The device showed the maximum transconductance of $g_m = 46$ mS mm^{-1}, the drain current of $I_D = 240$ mA mm^{-1}, and the on-resistance of $R_{ON} = 30\ \Omega$ mm. FLOSFIA Inc., a Japanese company, has been developing α-Ga_2O_3 devices using mist CVD for the growth of the active layers. The up-to-date data show the low on-resistance and large current SBDs and high reverse voltage of 1400 V of the pn junction.[43] It is expected that mist CVD contributes to the supply of low-cost α-Ga_2O_3 and β-Ga_2O_3 devices in the market.

ORCID iDs Hitoshi Takane https://orcid.org/0000-0001-8866-145X Jun Suda https://orcid.org/0000-0002-5453-4943
Katsuhisa Tanaka https://orcid.org/0000-0002-1409-2802
Shizuo Fujita https://orcid.org/0000-0001-6384-6693

1) S. J. Pearton, J. Yang, P. H. Cary, F. Ren, J. Kim, M. J. Tadjer, and M. A. Mastro, Appl. Phys. Rev. **5**, 011301 (2018).
2) A. J. Green et al., APL Mater. **10**, 029201 (2022).
3) E. G. Villora, K. Shimamura, Y. Yoshikawa, K. Aoki, and N. Ichinose, J. Cryst. Growth **270**, 420 (2004).
4) H. Aida, K. Nishiguchi, H. Takeda, N. Aota, K. Sunakawa, and Y. Yaguchi, Jpn. J. Appl. Phys. **47**, 8506 (2008).
5) K. Hoshikawa, E. Ohba, T. Kobayashi, J. Yanagisawa, C. Miyagawa, and Y. Nakamura, J. Cryst. Growth **447**, 36 (2016).
6) A. Kuramata, K. Koshi, S. Watanabe, Y. Yamaoka, T. Masui, and S. Yamakoshi, Jpn. J. Appl. Phys. **55**, 1202A2 (2016).
7) Z. Galazka, R. Uecker, D. Klimm, K. Irmscher, M. Naumann, M. Pietsch, A. Kwasniewski, R. Bertram, S. Ganschow, and M. Bickermann, ECS J. Solid State Sci. Technol. **6**, Q3007 (2017).
8) K. Sasaki, A. Kuramata, T. Masui, E. G. Víllora, K. Shimamura, and S. Yamakoshi, Appl. Phys. Express **5**, 035502 (2012).
9) H. Okumura, M. Kita, K. Sasaki, A. Kuramata, M. Higashiwaki, and J. S. Speck, Appl. Phys. Express **7**, 095501 (2014).
10) H. Murakami et al., Appl. Phys. Express **8**, 015503 (2015).
11) G. Wagner, M. Baldini, D. Gogova, M. Schmidbauer, R. Schewski, M. Albrecht, Z. Galazka, D. Klimm, and R. Fornari, Phys. Status Solidi A **211**, 27 (2014).
12) H. Zhou et al., IEEE Electron Device Lett. **40**, 1788 (2019).
13) C.-H. Lin et al., IEEE Electron Device Lett. **40**, 1487 (2019).
14) W. Li, K. Nomoto, Z. Hu, D. Jena, and H. G. Xing, Appl. Phys. Express **12**, 061007 (2019).
15) H. H. Gong, X. H. Chen, Y. Xu, F.-F. Ren, S. L. Gu, and J. D. Ye, Appl. Phys. Lett. **117**, 022104 (2020).
16) J. Zhang et al., Nat. Commun. **13**, 3900 (2022).
17) A. Bhattacharyya, S. Sharma, F. Alema, P. Ranga, S. Roy, C. Peterson, G. Seryogin, A. Osinsky, U. Singisetti, and S. Krishnamoorthy, Appl. Phys. Express **15**, 061001 (2022).
18) A. V. Dheenan, J. F. McGlone, N. K. Kalarickal, H. L. Huang, M. Brenner, J. Hwang, S. A. Ringel, and S. Rajan, Appl. Phys. Lett. **121**, 113503 (2022).
19) A. Bhattacharyya, S. Roy, P. Ranga, C. Peterson, and S. Krishnamoorthy, IEEE Electron Device Lett. **43**, 1637 (2022).
20) D. M. Dryden et al., IEEE Electron Device Lett. **43**, 1307 (2022).
21) S. Sharma, K. Zeng, S. Saha, and U. Singisetti, IEEE Electron Device Lett. **41**, 836 (2020).
22) T. Kamimura, Y. Nakata, and M. Higashiwaki, Appl. Phys. Lett. **117**, 253501 (2020).
23) X. Zhou, Y. Ma, G. Xu, Q. Liu, J. Liu, Q. He, X. Zhao, and S. Long, Appl. Phys. Lett. **121**, 223501 (2022).
24) D. Wakimoto, C.-H. Lin, Q. T. Thieu, H. Miyamoto, K. Sasaki, and A. Kuramata, Appl. Phys. Express **16**, 036503 (2023).
25) S. Krishnamoorthy et al., Appl. Phys. Lett. **111**, 023502 (2017).
26) E. Ahmadi, O. S. Koksaldi, X. Zheng, T. Mates, Y. Oshima, U. K. Mishra, and J. S. Speck, Appl. Phys. Express **10**, 071101 (2017).
27) Y. Zhang et al., Appl. Phys. Lett. **112**, 173502 (2018).
28) N. K. Kalarickal, Z. Xia, J. F. McGlone, Y. Liu, W. Moore, A. R. Arehart, S. A. Ringel, and S. Rajan, J. Appl. Phys. **127**, 215706 (2020).
29) T. Kawaharamura, H. Nishinaka, and S. Fujita, Jpn. J. Appl. Phys. **47**, 4669 (2008).
30) D. Shinohara and S. Fujita, Jpn. J. Appl. Phys. **47**, 7311 (2008).
31) T. Okuno, T. Oshima, S. D. Lee, and S. Fujita, Phys. Status Solidi C **8**, 540 (2011).
32) N. Suzuki, K. Kaneko, and S. Fujita, J. Cryst. Growth **364**, 30 (2013).
33) H. Takane and K. Kaneko, Appl. Phys. Lett. **119**, 062104 (2021).
34) S. D. Lee, K. Kaneko, and S. Fujita, Jpn. J. Appl. Phys. **55**, 1202B8 (2016).
35) H. Nishinaka, T. Nagaoka, Y. Kajita, and M. Yoshimoto, Mater. Sci. Semicond. Process. **128**, 105732 (2021).
36) T. Ogawa, H. Nishinaka, K. Shimazoe, T. Nagaoka, H. Miyake, K. Kanegae, and M. Yoshimoto, Jpn. J. Appl. Phys. **62**, SF1016 (2023).
37) M. Kaneko, H. Nishinaka, K. Kanegae, and M. Yoshimoto, Jpn. J. Appl. Phys. **62**, SF1002 (2023).
38) A. Bhattacharyya, C. Peterson, T. Itoh, S. Roy, J. Cooke, S. Rebollo, P. Ranga, B. Sensale-Rodriguez, and S. Krishnamoorthy, APL Mater. **11**, 021110 (2023).
39) M. Passlack, E. F. Schubert, and W. S. Hobson, J. Appl. Phys. **77**, 686 (1995).
40) S. Kumar, T. Kamimura, C. H. Lin, Y. Nakata, and M. Higashiwaki, Appl. Phys. Lett. **117**, 193502 (2020).
41) M. H. Wong, K. Sasaki, A. Kuramata, S. Yamakoshi, and M. Higashiwaki, Appl. Phys. Lett. **106**, 032105 (2015).
42) K. Konishi, K. Goto, R. Togashi, H. Murakami, M. Higashiwaki, A. Kuramata, S. Yamakoshi, B. Monemar, and Y. Kumagai, J. Cryst. Growth **492**, 39 (2018).
43) K. Kaneko, S. Fujita, T. Shinohe, and K. Tanaka, Jpn. J. Appl. Phys. **62**, SF0803 (2023).